

See discussions, stats, and author profiles for this publication at: <https://www.researchgate.net/publication/310780093>

Evaluation of the WRF-lake model over a highland freshwater lake in southwest China: Evaluation of the WRF-lake model

Article in *Journal of Geophysical Research Atmospheres* · November 2016

DOI: 10.1002/2016JD025396

CITATIONS

3

READS

144

4 authors, including:



Huizhi Liu

Institute of Atmospheric Physics

75 PUBLICATIONS 869 CITATIONS

[SEE PROFILE](#)

Some of the authors of this publication are also working on these related projects:



The NSFC project(40675052)- 中国科学院寒区旱区环境与工程研究所
[View project](#)

Journal of Geophysical Research: Atmospheres

RESEARCH ARTICLE

10.1002/2016JD025396

Key Points:

- Eddy diffusivity is small in the surface layer when there is thermal stratification
- Lake surface temperature is more sensitive to surface roughness length and eddy diffusivity than water clarity
- Topographic correction improves simulations of surface heat fluxes over complex mountainous terrain

Correspondence to:H. Liu,
huizhil@mail.iap.ac.cn**Citation:**

Xu, L., H. Liu, Q. Du, and L. Wang (2017), Evaluation of the WRF-lake model over a highland freshwater lake in southwest China, *J. Geophys. Res. Atmos.*, 121, 13,989–14,005, doi:10.1002/2016JD025396.

Received 22 MAY 2016

Accepted 19 NOV 2016

Accepted article online 23 NOV 2016

Published online 15 DEC 2016

Evaluation of the WRF-lake model over a highland freshwater lake in southwest China

Lujun Xu^{1,2} , Huizhi Liu¹ , Qun Du¹, and Lei Wang¹

¹State Key Laboratory of Atmospheric Boundary Layer Physics and Atmospheric Chemistry, Institute of Atmospheric Physics, Chinese Academy of Sciences, Beijing, China, ²College of Earth Sciences, University of Chinese Academy of Sciences, Beijing, China

Abstract Evaluation of the Weather Research and Forecasting Model version 3.7.1 lake model performance on lake physical processes and lake-atmosphere interaction at Erhai Lake was conducted with in situ observation data sets over the lake to verify the model results. The lake model with default parameters presented significant negative bias during the day and positive bias during the night on lake surface temperature. Calibrations of water absorption and extinction coefficients, surface roughness length, and eddy diffusion coefficient were carried out to correct this bias. The added absorption and extinction coefficients increased solar radiation in upper water layer, leading to a little higher surface temperature. Compared to constant surface roughness lengths, parameterization of roughness lengths as functions of friction velocity and fetch length significantly improved simulations of lake surface temperature and sensible heat flux. In Erhai Lake, eddy diffusion coefficient of the Henderson-Sellers parameterization is smaller than that in deep lakes. The eddy diffusion coefficient was reduced by a factor of 0.05 in dry season and 0.02 in wet season, respectively, to restrict mixing strength, generating a reasonable diurnal range with observed surface temperature. The adjusted parameter simulations matched better with in situ observations in diurnal cycle of temperature and surface heat fluxes but still overestimated wind speed. Topographic correction is effective to correct the bias, indicating that topographic correction over complex terrain was necessary.

1. Introduction

Lake-atmosphere interactions have significant impacts on local climate, acting as indicators of climate changes [Adrian *et al.*, 2009]. Due to low albedo, high heat capacity, and low surface roughness, lakes perform differently from other land surfaces in momentum, water vapor exchange, and energy budgets [Bonan, 1995]. This results in spatial heterogeneity of radiation, temperature, and surface turbulent fluxes in regions where lakes cover a large fraction of the Earth surface [Stepanenko *et al.*, 2013]. Compared to surrounding land surfaces, lakes tend to reduce diurnal temperature range [Samuelsson *et al.*, 2010]. Lakes in low latitude which are characterized by high surface temperature increase latent heat flux [Curtarelli *et al.*, 2014]. What is more, the lake-land contrast at diurnal scale leads to lake-land breeze circulation, which changes local wind field and even mesoscale flow [Samuelsson and Tjernstrom, 2001]. Lake breeze can interact with topography and background wind and induce moist and deep convection [Gerken *et al.*, 2014]. Lake physics and biochemistry properties also respond to climate changes. Changes of climate affect lake mixing and nutrient, which have a direct influence on heat storage and evaporation, resulting in area, depth, salinity, and biology changing of lakes [Verburg and Hecky, 2009].

The importance of lake-atmosphere interaction has been indicated in numerical investigations including sub-grid parameterization of lakes [Petenko *et al.*, 2011; Gerken *et al.*, 2014]. With enhancing of weather forecast and climate models' resolution, lakes have become an essential underlying surface as numerical models allow lakes to be explicitly resolved. Numerical weather prediction models provide atmospheric forcing for lake models and receive surface momentum, water, and heat fluxes from lake models as boundary conditions. The lake models range from one-dimensional (1-D) bulk formulation model [Goyette *et al.*, 2000] to complicated three-dimensional (3-D) turbulence model [Pan *et al.*, 2002; Long *et al.*, 2007]. According to their physically based parameterizations, lake models can be typically classified into two categories: finite difference models (e.g., the Hostetler model [Hostetler and Bartlein, 1990] and SIMSTRAT [Goudsmit *et al.*, 2002]) and bulk formulation models (e.g., FLake [Mironov *et al.*, 2010]). The former uses finite difference technique to solve the heat transport equation. The eddy transfer is calculated by employing the Richardson number or turbulence closure equations [Joehnk and Umlauf, 2001]. The latter is based on experiential temperature profile and on integral energy in a slab of depth. The finite difference models allow the reproduction of

mixing process. However, they are computationally expensive than bulk lake models. Bulk models perform reasonably surface temperature. But they encounter difficulties in simulating stratification and water temperature at deep depth of lake. The Lake Model Intercomparison Project from 2008 demonstrates advantages and limitations of those lake models using observations of a great many lakes over the world, representing different mixing regimes and climate conditions [Stepanenko *et al.*, 2010]. It is a significant step before lake models are used for weather and climate prediction models. Due to physics adequacy and numerical efficiency, 1-D lake models have usually been employed to couple into regional and global climate models [Tantzap *et al.*, 2007; Bartunkova *et al.*, 2014]. Researches have proved that 1-D lake models are feasible for a wide range of lakes [Mironov *et al.*, 2010; Stepanenko *et al.*, 2013; Thiery *et al.*, 2014].

The Weather Research and Forecasting Model version 3.7.1 (WRFv3.7.1) has recently included the Community Land Model (CLM) lake model, which is based on the Hostetler model [Skamarock *et al.*, 2008]. The off-line lake model reproduces water temperature on diurnal cycle at the Taihu Lake [Deng *et al.*, 2013]. However, performance of the coupled WRF-CLM lake model is still unclear. In this study, we aim at evaluating performance of the WRF lake model at Erhai Lake using observational data and investigate physical processes of lake-atmosphere interaction. Topographic correction was also conducted in order to improve description of lake-atmosphere interactions.

The Erhai Lake is chosen for two reasons. First, previous researches in China have focused on lake-atmosphere interaction processes over large lakes, such as the Nam Co Lake [Haginoya *et al.*, 2009], the Tai Lake [Wang *et al.*, 2014], and the Ngoring Lake [Li *et al.*, 2015]. There is little information on lake-atmosphere interaction of moderate and small lakes in China [Hu *et al.*, 2015; Wang *et al.*, 2015]. There are about 2666 moderate and small lakes in China, covering an area of nearly 46,895.2 km² [Ma *et al.*, 2011]. The Erhai Lake is a highland open water of medium size in low latitude. A long-term observation site has been established over the lake since 2011, providing database for validation of numerical simulations. Second, the Erhai Lake locates in the middle of the Dali Basin, in the joint of the Yun-Gui Plateau and the Hengduan Mountains, the southeast edge of the Tibetan Plateau. The mountain blocking effect allows establishing of local circulation and microclimate. Due to the unique geography and climate environment, lake-atmosphere interaction processes and local circulation in the Erhai Lake have its own characteristics [Xu *et al.*, 2016]. Although the lake is 1972 m above mean sea level, it is ice free throughout the year and shows no seasonal thermal structure. The synoptic current interacts with the local valley circulation and the lake-land circulation in this area. A validated WRF-lake model aid to analyze physical processes of lake-atmosphere interaction and local microclimate over open freshwater lake in mountain area.

2. Site and Data

The Erhai Lake situates at the southeastern edge of the Tibetan Plateau in the Dali Basin of Yunnan Province, southwest China. It covers a surface area of more than 250 km². The major axis is about 42.6 km long, going from northwest to southeast, and the maximum width is approximately 9 km. The depth of the lake is nearly 10.2 m on average, with a maximum depth of 21.7 m. The lake is 13 km away from the Cangshan Mountain in the west. The climate in Erhai area is a low-latitude plateau monsoon climate, with an obvious warm-wet season (May to October) and a cold-dry season (November to April of the next year). The Erhai Lake is ice free all the year around. When compared with other lakes in low elevation, Erhai Lake does not show obvious thermal stratification [Deng *et al.*, 2013; Feng *et al.*, 2016]. It receives water from streams in the east, the Boluo River in the southeast, 19 streams from the Cangshan Mountains in the west, and the Miju River in the north. The only outlet is the Xier River in the southwest.

A fixed platform with 80 m away from the shore is nearly 1–2 m above the water surface. The measurements include an open-path eddy covariance system, the shortwave and longwave radiation, and the meteorological observation system. The postprocessing software is EddyPro 4.0. Water temperature at depths of 15 cm, 35 cm, 65 cm, 115 cm, 215 cm, 415 cm, 615 cm, and 815 cm are measured by CS616 (thermal couple). More measurement details are described in the paper by Liu *et al.* [2015].

3. Method

3.1. Lake Model

The Community Land Model version 4.5 [Oleson *et al.*, 2013] lake model, denoting the Lake, Ice, Snow, and Sediment Simulator, had been coupled into the Weather Research and Forecasting (WRF) model in version

3.7.1. It contains a 1-D thermal diffusion lake scheme, which is modified by *Gu et al.* [2015]. Actual lake depth can be employed in the lake scheme. The physical process is based on *Hostetler and Bartlein* [1990], *Bonan* [1995], and *Subin et al.* [2012]. We evaluated the model performance at Erhai Lake and clarify the effect of important processes on lake heat and water budgets with different parameter sets.

For ice-free lake, energy transport can be divided into two parts: surface layer heat exchange and subsurface layer heating. The surface layer is responsible for the transfer of momentum, heat flux, and water vapor between the lake and the atmosphere. The energy balance equation of the surface layer is given by

$$\beta(K_{\downarrow} - K_{\uparrow}) + (L_{\downarrow} - L_{\uparrow}) = Q_H + Q_E + Q_G, \quad (1)$$

where K_{\downarrow} and K_{\uparrow} are the incoming and outgoing shortwave radiation (W m^{-2}), L_{\downarrow} and L_{\uparrow} are the incoming and outgoing longwave radiation (W m^{-2}), Q_H is the sensible heat flux (W m^{-2}), Q_E is the latent heat flux (W m^{-2}), and Q_G is the heat storage term (W m^{-2} ; positive toward the atmosphere). The lake surface layer absorbs part of net shortwave radiation, which is set as β , and the rest penetrates and is absorbed by subsurface layers following the Beer-Lambert law. According to *Oleson et al.* [2013], the visible wave band ($< 0.7 \mu\text{m}$) penetrates and the near-infrared wave band ($\geq 0.7 \mu\text{m}$) is absorbed by the surface layer. The lake model assumes water to be limpidity, 40% of net solar radiation is absorbed in the surface layer, which is equal to the near-infrared fraction. And 60% of net solar radiation penetrates and decayed by an extinction coefficient η , as it is absorbed and scattered by the underlying water.

For the surface layer, surface temperature T_g ($^{\circ}\text{C}$) of the first time step is received from atmosphere boundary layer, and the next time step temperature is calculated by

$$\Delta T_g = \frac{(K_{\downarrow} - K_{\uparrow}) - (L_{\uparrow} - L_{\downarrow}) - Q_H - Q_E - Q_G}{\frac{\partial(L_{\uparrow} - L_{\downarrow})}{\partial T_g} + \frac{\partial Q_H}{\partial T_g} + \frac{\partial Q_E}{\partial T_g} + \frac{\partial Q_G}{\partial T_g}}, \quad (2)$$

When the surface temperature T_g is solved, the momentum, heat, and water vapor fluxes are solved simultaneously. In the calculation of turbulence heat fluxes, for ice-free lakes, the model sets the aerodynamic roughness length (z_{0m}) to be 0.001 m, the value of roughness length for sensible heat and latent heat (z_{0h} and z_{0q}) equal to that of the momentum roughness length (z_{0m}).

For subsurface layers, lake temperature T ($^{\circ}\text{C}$) is governed by

$$\frac{\partial T}{\partial t} = \frac{\partial}{\partial z} \left[(K_m + K_e) \frac{\partial T}{\partial z} \right] + \frac{1}{c_{\text{liq}}} \frac{d\emptyset}{dz}, \quad (3)$$

where K_m is the molecular diffusion coefficient ($\text{m}^2 \text{s}^{-1}$), K_e is the eddy diffusion coefficients ($\text{m}^2 \text{s}^{-1}$), c_{liq} is the volumetric heat capacity of water ($\text{J kg}^{-1} \text{K}^{-1}$), z is the depth from the surface (m), and \emptyset is the subsurface solar radiation heat source term (W m^{-2}).

$$\emptyset = (1 - \beta(K_{\downarrow} - K_{\uparrow})) \exp(-\eta(z - z_a)), \quad (4)$$

where $\eta = 1.1925d^{-0.424}$ is the light extinction coefficient, d is the lake depth, and z_a is the thickness of the surface layer (m).

The wind-driven eddy diffusion coefficient K_e for layer i is

$$K_e = \begin{cases} \frac{1.2 \times 10^{-3} u_2 k z_i}{P_0 (1 + 37 R_i^2)} \exp(-k^* z_i) & T_g > T_f \\ 0 & T_g \leq T_f \end{cases}, \quad (5)$$

where i is the layer index ($1 \leq i \leq 10$), $k = 0.4$ is the von Karman constant, u_2 is the 2 m wind speed (m s^{-1}), z_i is the node depth (m), P_0 is the neutral value of the turbulent Prandtl number, R_i is the gradient Richardson number, $k^* = 6.6 u_2^{-1.84} \sqrt{|\sin \emptyset|}$, and T_f is the freezing temperature of water ($^{\circ}\text{C}$).

3.2. Setup of Model Simulations

The WRF model was driven by the National Centers for Environmental Prediction final operational global analysis and forecast data with 6 h temporal resolution and $1^{\circ} \times 1^{\circ}$ spatial resolution as initial and boundary conditions. The terrain data were derived from the WRF Preprocessing System Geographical Input data. Two-way nesting with three domains with horizontal resolutions of 9 km, 3 km, and 1 km, respectively, was

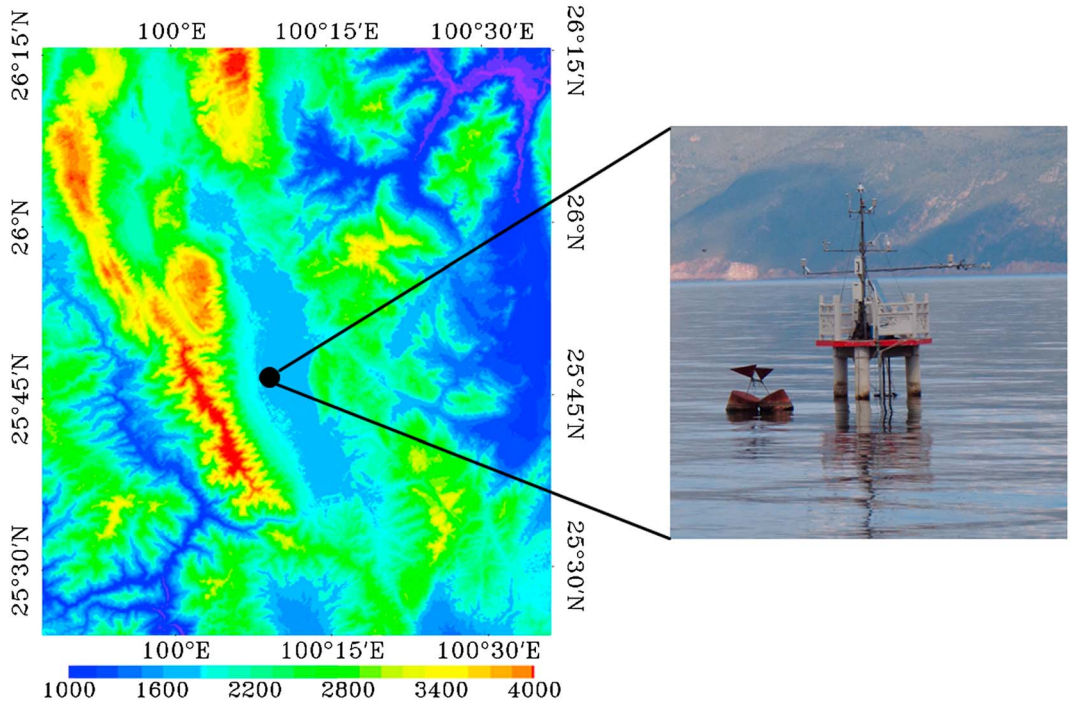


Figure 1. Topographic height (units: m) of the innermost region and observation site over Erhai Lake.

employed. The domains were centered at the observation site (25.7°N , 100.15°E), consisting of 60×80 , 70×91 , and 100×100 grids, respectively. The topography of the innermost layer is shown in Figure 1. The main physical parameterization schemes are shown in Table 1. The cumulus parameterization was only conducted for 9 km, and no explicit cumulus scheme was adopted in the domains with horizontal resolution of 3 km and 1 km.

There are two seasons (wet season and dry season) in Erhai area each year. Sensitivity experiments were conducted during typical period of each season. The simulation period of sensitivity experiments ranged from 0800 3 August to 0800 19 August (CST (Chinese Standard Time, UTC+8)) 2012 in wet season and 0800 30 November to 0800 15 December (CST) 2012 in dry season. The first 7 days were spin-up time for removing effect of initial conditions. There was no synoptic process during the selected period in dry season. We subjected this case to a thorough evaluation and sensitivity analysis. In wet season, the northwest Pacific Subtropical High (STH) controls most of the rainfall in Erhai area. The selected period in wet season covered a westward extension process of the STH, bringing precipitation at Erhai area.

The absorb fraction of net solar radiation in the surface layer depends partly on the location and turbidity of lakes. The extinction coefficient η depends largely on water quality. In this study, the extinction coefficient was set based on observations in different seasons. The absorption coefficient is difficult to quantify by measurement. Deng *et al.* [2013] related absorption coefficient β to extinction coefficient η according to the Beer-Lambert law as $\beta = 1 - e^{-z_a\eta}$, where z_a is the surface layer thickness. In this study, we used Deng *et al.* [2013]'s formula.

The roughness length is a key parameter for coupling between the lake and the atmosphere. It determines exchanging of momentum, heat, and water vapor. In sensitivity tests, z_0 is given by Subin *et al.* [2012] as following

$$z_{0m} = \max\left(\frac{\alpha v}{u_*}, \frac{cu_*^2}{g}\right), \quad (6)$$

$$z_{0h} = z_{0m} \exp\left(-\frac{\kappa}{P_r} (4\sqrt{R_0} - 3.2)\right), \quad (7)$$

$$z_{0q} = z_{0m} \exp\left(-\frac{\kappa}{S_c} (4\sqrt{R_0} - 4.2)\right), \quad (8)$$

Table 1. Model Settings

Model Property	Description
Model version	WRF model 3.7.1
Nesting	Two-way nesting
Microphysics	Lin et al. [Lin and Jao, 1995]
Longwave radiation	RRTM [Mlawer et al., 1997]
Shortwave radiation	Dudhia [Dudhia, 1989]
Land surface	Noah [Chen and Dudhia, 2001]
Boundary layer	YSU [Hong et al., 2006]
Cumulus scheme	Grell-Devenyi [Grell and Devenyi, 2002]
Urban surface	Urban canopy model [Masson, 2000]
Lake scheme	CLM 4.5 lake model [Oleson et al., 2013]

where $\alpha=0.1$ is a dimensionless empirical constant, u_* is the friction velocity in the surface layer (m s^{-1}), v is the kinematic viscosity of air ($\text{m}^2 \text{s}^{-1}$) as given below, c is the effective Charnock coefficient as given below, g is the acceleration of gravity (m s^{-2}), $k=0.4$ is the von Karman constant, $P_r=0.71$ is the Prandtl number for air, R_0 is the near-surface atmospheric roughness Reynolds number as given below, and $S_c=0.66$ is the Schmidt number for water in air.

$$v = v_0 \left(\frac{T_g}{T_0} \right)^{1.5} \frac{P_0}{P}, \quad (9)$$

where $v_0=1.51 \times 10^{-5} \text{ m}^2 \text{s}^{-1}$, T_g is the ground surface temperature, $T_0=293.15 \text{ K}$ is the standard temperature, $P_0=1.013 \times 10^5 \text{ Pa}$ is the standard pressure, and P is the atmospheric pressure at the reference height.

$$c = c_{\min} + (c_{\max} - c_{\min}) \exp \left(-\min \left(\frac{\left(\frac{F_g}{u_*^2} \right)^{\frac{1}{3}}}{f_c}, \varepsilon \frac{\sqrt{dg}}{u_*} \right) \right), \quad (10)$$

where $c_{\min}=0.01$, $c_{\max}=0.11$, $F=25$ d is the fetch (m), d is the lake depth, and $\varepsilon=1$ in this study.

$$R_0 = \max \left(0.1, \frac{z_{0m} u_*}{v} \right), \quad (11)$$

The eddy diffusion parameterization originates from Hostetler and Bartlein [1990]. According to the study of Gu et al. [2015], when increasing the eddy diffusivity (ke) by 10^5 for large and deep lakes, the model could predict the surface temperature more accurately. For shallow lakes, it might be excessively mixed [Subin et al., 2012]. In sensitivity tests, we scaled down ke by 0.05 and 0.02 in dry season and wet season, respectively. Details of parameter setting in sensitivity tests were shown in Tables 2 and 3.

4. Results

4.1. Sensitivity Tests in Dry Season

4.1.1. Radiation Parameterization Schemes

Solar radiation is the driving force of momentum, heat, and water vapor fluxes between the atmosphere and the underlying surface. Radiation scheme has significant influence on model simulation results [Ruiz-Arias et al., 2016]. Before evaluating model performance on lake surface temperature, four radiation parameterization schemes were performed at the Erhai Lake, which are Dudhia shortwave and rapid radiative transfer model longwave, National Center for Atmospheric Research Community Atmosphere Model shortwave and longwave [Collins et al., 2004], rapid radiative transfer model for general circulation model (RRMTG)

Table 2. Lake Parameter Setting for Different Cases in Dry Season

Case	Absorption Coefficient	Extinction Coefficient (Units: m^{-1})	Surface Roughness (Units: m)	Eddy Diffusion Coefficient (Units: $\text{m}^2 \text{s}^{-1}$)
a	0.4	0.45	0.001	ke
b	0.4	0.45	parameterization	ke
c	0.4	0.45	0.001	$0.05 \times ke$
d	0.4	0.45	parameterization	$0.05 \times ke$
1	0.6	1.1	0.001	ke
2	0.6	1.1	parameterization	ke
3	0.6	1.1	0.001	$0.05 \times ke$
4	0.6	1.1	parameterization	$0.05 \times ke$

Table 3. Lake Parameter Setting for Different Cases in Wet Season

Case	Absorption Coefficient	Extinction Coefficient (Units: m^{-1})	Surface Roughness (Units: m)	Eddy Diffusion Coefficient (Units: $m^2 s^{-1}$)
a	0.4	0.45	0.001	ke
b	0.4	0.45	parameterization	ke
c	0.4	0.45	0.001	$0.02 \times ke$
d	0.4	0.45	parameterization	$0.02 \times ke$
1	0.76	2.4	0.001	ke
2	0.76	2.4	parameterization	ke
3	0.76	2.4	0.001	$0.02 \times ke$
4	0.76	2.4	parameterization	$0.02 \times ke$

shortwave and longwave [Iacono and Nehrkorn, 2010], and New Goddard shortwave and longwave [Chou and Suarez, 1999] radiation parameterization schemes.

It appears that the four schemes reproduced total solar radiation well on clear days (Figure 2a). But there was bias with clouds existing. None of these configurations captured clouds' effects on solar radiation in 8 and 13 December, while Community Atmosphere Model version 3 (CAM3), RRTMG, and New Goddard could simulate the clouds' effects on 9 December. It resulted in positive bias of shortwave radiation at noon. The mean bias (MB) of the Dudhia, CAM, RRTMG, and New Goddard shortwave radiation scheme for the simulation period were 25.6, 31.5, 29, and 31.9 $W m^{-2}$, respectively. The mean absolute error (MAE) of each shortwave radiation scheme was 38.6, 39.9, 37.9, and 41.3 $W m^{-2}$, respectively. For downward longwave radiation simulations, four schemes show negative bias. The MB of the RRTM, CAM, RRTMG, and New Goddard longwave radiation scheme were -6.5 , -12.7 , -7.7 , and $-16.6 W m^{-2}$, respectively. The MAE in the New Goddard longwave radiation scheme was the largest in the four schemes ($-23.6 W m^{-2}$), while the RRTMG scheme slightly improved the overall bias ($-16.6 W m^{-2}$ and $-16.9 W m^{-2}$ for RRTM and $-19 W m^{-2}$ for CAM). The bias is mainly related to misrepresentations of clouds and aerosols [Oreopoulos et al., 2012]. It resulted in a 0.2 (0.75), 0.25 (0.8), 0.2 (0.7), and 0.26 (0.82) $^{\circ}C$ MB (MAE) of lake surface temperature for the Dudhia, CAM, RRTMG, and New Goddard radiation schemes, respectively. Compared with different schemes, we use the RRTMG scheme for latter simulations due to a slightly better representation of downward shortwave and longwave radiation.

4.1.2. Initial Simulation for Erhai Lake

In this study, we focus on the lake surface temperature, as it is the key variable driving the sensible and latent heat fluxes exchanging between the water surface and the atmosphere. During our simulation period (30 November to 15 December 2012), the surface temperature of Erhai Lake ranged from $12^{\circ}C$ to $18^{\circ}C$, which was warmer than deep lake [Haginoya et al., 2009]. The lake was warmer than the atmosphere, serving as a heat source since August. Default parameter of the lake model failed to reproduce lake surface temperature as shown in Figure 3a. The simulated lake surface temperature was lower than the observation during the day. It was partly because the surface layer absorbed less radiation to heat surface water and transferred

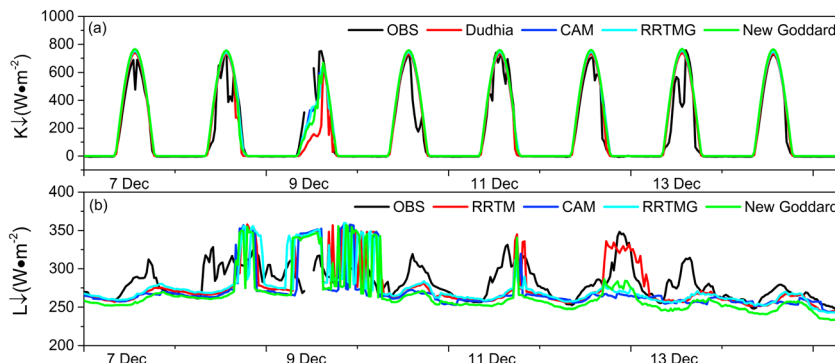


Figure 2. Time series of simulations (four radiation schemes) and observations of (a) downward shortwave radiation and (b) downward longwave radiation (units: $W m^{-2}$).

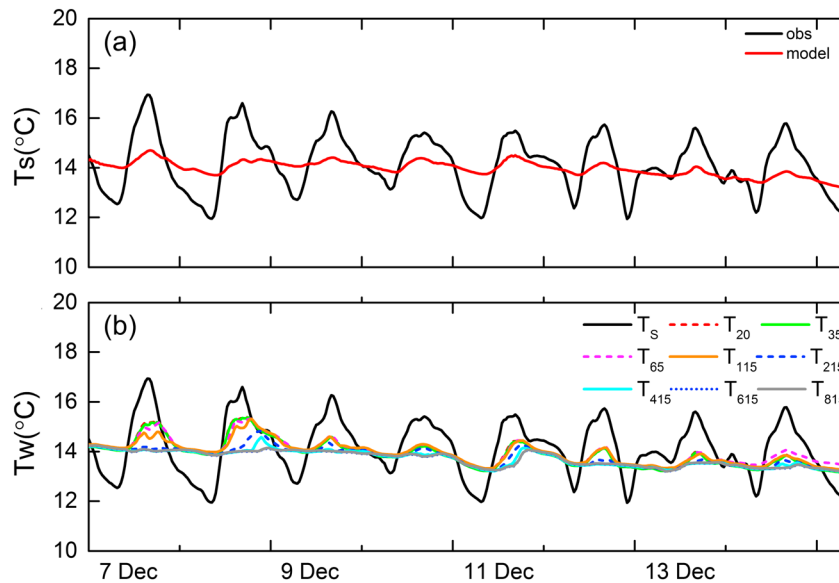


Figure 3. (a) Lake surface temperature of initial simulation (red line) and observation (black line) and (b) water temperature measurements; the number in the subscript denotes the measurement depth (cm) (units: °C).

more radiation into deeper water. At night, the simulated lake surface temperature was higher than observations. The turbulent mixing is strong for Erhai Lake during night, leading to disappearance of the thermal stratification, which is different from the observation in Figure 3b. The correlation coefficient was only 0.35 between the simulated and observed lake surface temperatures (LSTs).

The drivers of lake heat and water vapor exchange processes include the absorb fraction of net solar radiation in the surface layer, solar light extinction coefficient, the surface roughness length, the eddy diffusion coefficient, and others. We calibrated the WRF lake model with adjustment of the absorption and extinction coefficients, the surface roughness length, and the eddy diffusion coefficient in this paper.

4.1.3. Calibration Simulations

Sensitivity tests were conducted in dry season to simulate lake-air interaction. The model assumed lakes to be clear. In fact, the Erhai Lake is eutrophicated due to human being's activities and water pollution. The amount of nutrients can limit and control light diffusion, resulting in more radiation retains in the upper layer and less radiation transfers to the deep water. For Nordic waters like the Tämnaren Lake, 42% of the solar radiation retain in the surface layer [Elo, 2007]. For the Taihu Lake, 80% are absorbed by the upper layer, since the Taihu Lake is seriously polluted [Gu et al., 2013]. Gu et al. [2013] enlarged the extinction coefficient η by 3 times to deal with high concentrations of suspended nutrients in the Taihu Lake. The Erhai Lake is in the process from moderate nutrition to eutrophication due to the urbanization of this area. In dry season, the Secchi depth of the Erhai Lake is 1.3 m, and the mean spectral absorption coefficient is 1.1 m^{-1} [Zhang et al., 2009], which is less than that of the Taihu Lake. Here we set η equal to 1.1 m^{-1} and $\beta = 1 - e^{-z_0\eta}$ with a value of nearly 0.6 in Figure 4b. The lake surface temperature increased by nearly 0.5°C . It came to the same physical behavior as for the Kuivajärvi Lake, in which lake surface temperature got higher with an increased extinction coefficient when there was no overturn [Heiskanen et al., 2015]. But there was still large negative bias in surface temperature simulation (Figure 5).

In case b, the tuned simulations of z_0 improved model performance significantly. The root-mean-square error (RMSE) of lake surface temperature decreased from 1.37°C (case a) to less than 1.05°C (case b). The lake was warmer than the atmosphere above during the simulated period. Without calibration of z_0 , the simulated LST was colder than the air, resulting in negative sensible heat flux (Figure 6). The latent heat flux was too large due to strong mechanical mixing with default z_0 (Figure 7). In cases with the tuned z_0 , the modeled sensible heat flux was consistent with observations. The diurnal timing of peak in sensible heat flux and latent heat flux were well reproduced. The modeled latent heat flux was higher than observations. The reason for this was that the simulated wind was large over complex terrain.

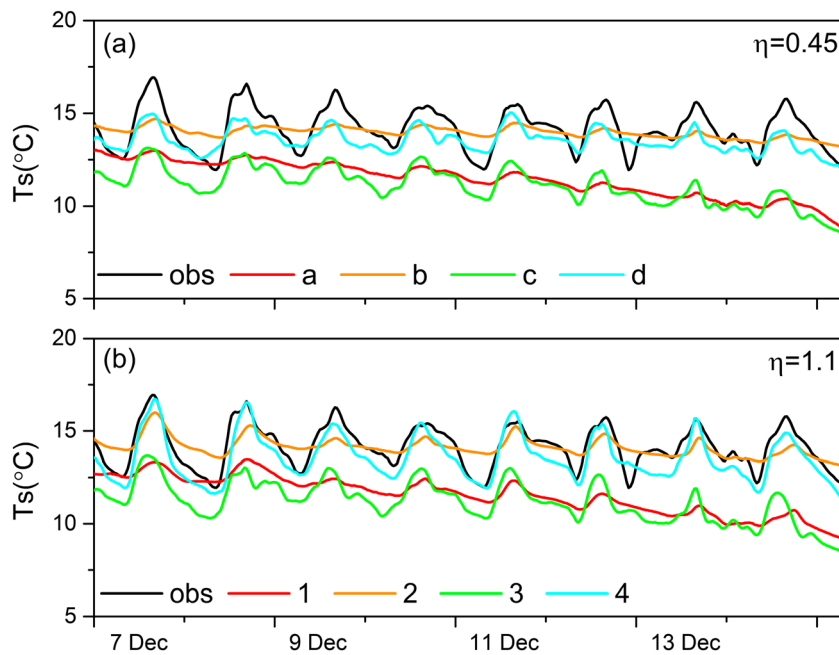


Figure 4. (a and b) Lake surface temperature comparison for observation (obs) and simulations of different model parameter setting in Table 2 (units: $^{\circ}\text{C}$).

As shown in Figure 8, the observed stratification was not reproduced by the default ke . The simulated lake temperature appeared uniform in the vertical. The diurnal variation of LST was smaller than that of the observation. The Erhai Lake is stratified within the upper 20 cm (Figure 3b). We decreased the eddy diffusivity within 20 cm by 0.05 to impose restrictions on mixing strength. The tuned ke varied from 0.1 to $5 \times 10^{-5} \text{ m}^2 \text{ s}^{-1}$, which was 2 orders of magnitude greater than the molecular diffusivity. It was in agreement with the range of ke in the Taihu Lake [Deng et al., 2013]. The simulated surface temperature matched the observation well (Figure 4b, case 4). The tuned ke improved surface temperature during the day. The surface layer absorbed radiation and got warmer in the day, resulting in stable stratification, which confined turbulent mixing. At night, the surface layer released the stored heat to the overlying atmosphere and became cooler than underlying water. The tuned ke reduced heat that compensated from deep water to the surface (Figure 8c). The correlation coefficient increased from 0.35 to 0.95, and the RMSE reduced from 1.35°C to 0.4°C (Figure 5b). By the combination of the added absorption and extinction coefficients, the parameterization of surface roughness length, and the reduced eddy diffusion coefficient, the model reproduced the correct diurnal cycle of LST (Figure 9).

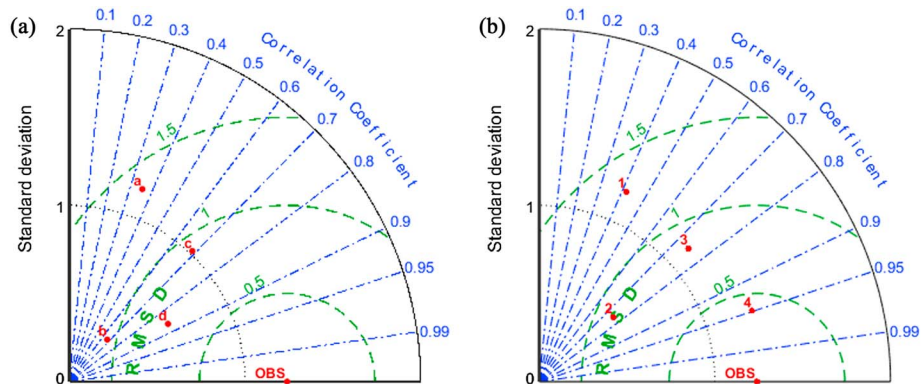


Figure 5. (a and b) Taylor diagram of lake surface temperature for observation (obs) and simulations of different model parameter setting in Table 2.

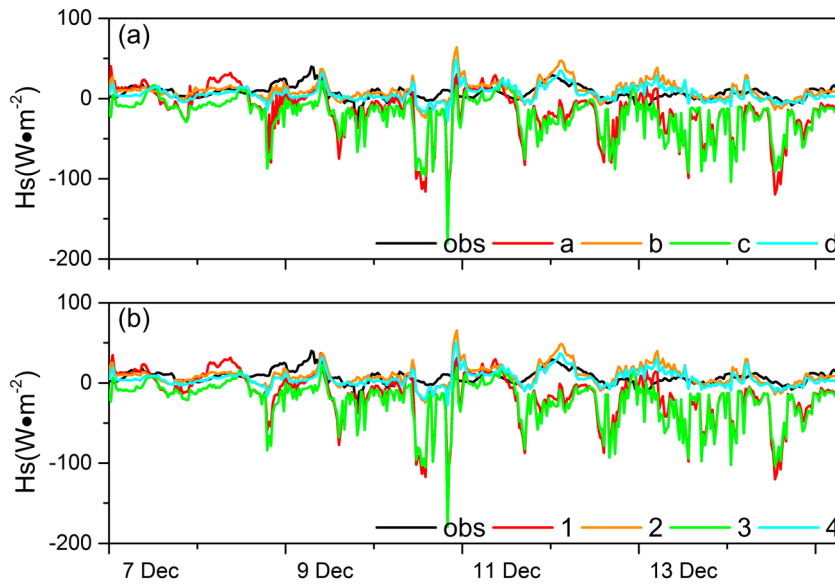


Figure 6. (a and b) Sensible heat flux comparison for observation (obs) and simulations of different model parameter setting in Table 2 (units: W m^{-2}).

4.2. Sensitivity Tests in Wet Season

In wet season, the cyanobacterial bloomed and the biomass of phytoplankton reached a high level, leading to a mesotrophic status lake [Chen *et al.*, 2015]. Nearly 90% of solar radiation are absorbed within a depth of 2 m [Haginoya *et al.*, 2012]. The surface layer absorption got higher and the extinction coefficient was 2.4 m^{-1} . Wind speed was less in summer and autumn than that in winter and spring, leading to a decreasing of the eddy diffusivity by 0.02 in wet season. Parameter setting for eight sensitivity tests was shown in Table 3. Statistic results of these tests were demonstrated by Taylor diagram in Figure 10.

The diurnal range of LST was 6.9°C during the period shown in Figure 11. It was larger than the diurnal range at the Taihu Lake (3.5°C) [Deng *et al.*, 2013]. The large diurnal range at the Erhai Lake was partly due to higher solar radiation at plateau than that at plain. Additionally, LST at the Erhai Lake was measured with a

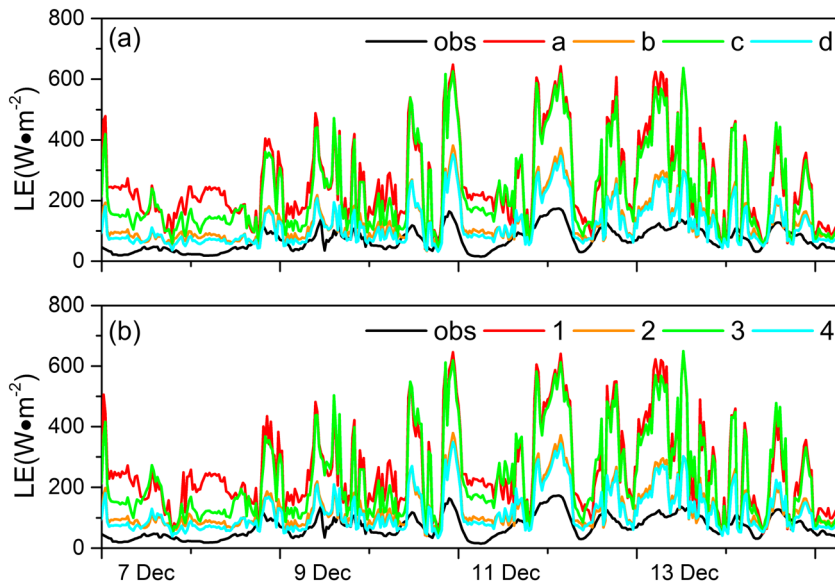


Figure 7. (a and b) Latent heat flux comparison for observation (obs) and simulations of different model parameter setting in Table 2 (units: W m^{-2}).

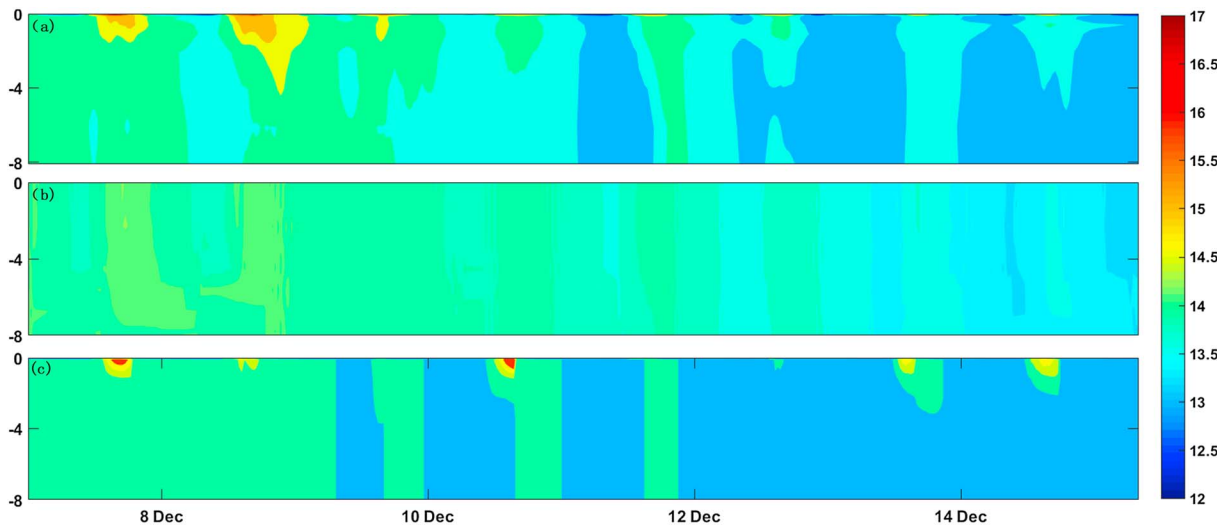


Figure 8. Water temperature comparison of (a) observed temperature, (b) water temperature predicted by default parameters, and (c) water temperature predicted by tuned parameters (case 4) (units: °C).

pyrgeometer, which got higher diurnal range than thermometer measured at a shallow depth of water. In case a, the diurnal range of LST was reduced by 5.7°C (Figure 9a). The default settings allowed more solar radiation to transfer into deeper water, and the stored energy was released at night. The LST increased as a response to worse water quality (Figure 9b). It was caused by decreasing the effective mixing depth and increasing thermal stratification [Subin *et al.*, 2012]. Heiskanen *et al.* [2015] found that thermal stratification of lake depended strongly on water clarity. Variation in water quality did not show measurable variation in surface heat fluxes. Fixing the roughness lengths caused about a 1°C increase of LST in the whole simulation period, at the expense of sensible and latent heat fluxes (Figures 11 and 12). This effect was magnified when ke within 20 cm was declined by 0.02 (Figures 11 and 12). By scaling down ke in the surface layer, the simulated LST matched closely with the observation (Figure 9b, case 4). The decreased ke reduced mixing and

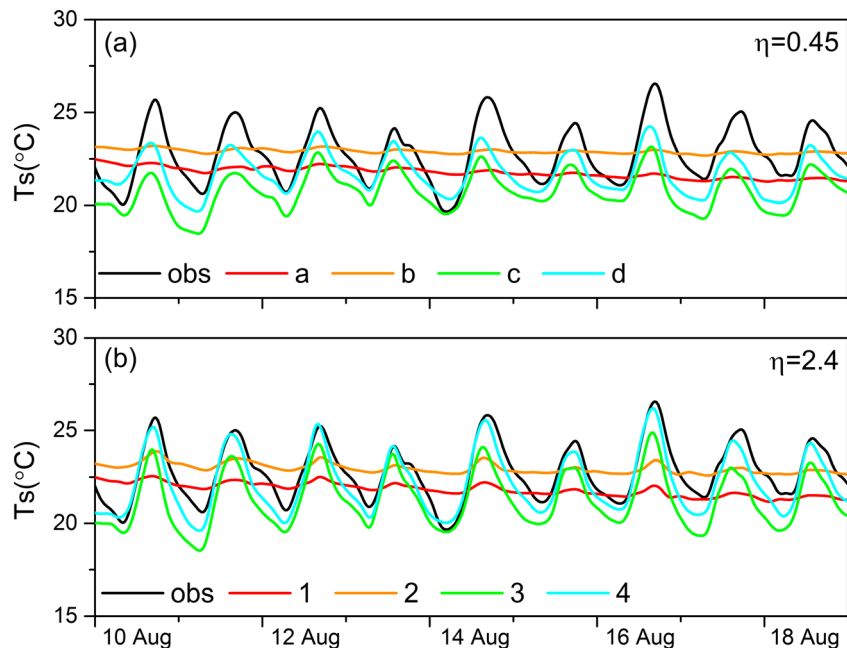


Figure 9. (a and b) Lake surface temperature comparison for observation (obs) and simulations of different model parameter setting in Table 3 (units: °C).

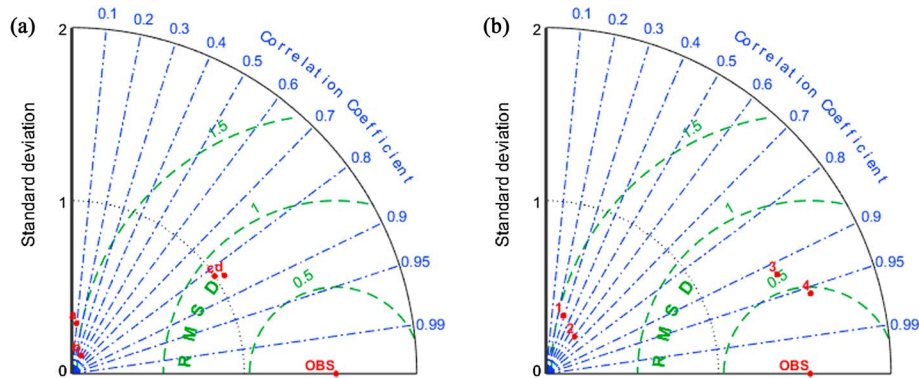


Figure 10. (a and b) Taylor diagram of lake surface temperature for observation (obs) and simulations of different model parameter setting in Table 3.

promoted the process of thermal stratification in the surface layer, resulting in less turbulent heat losses. The correlation coefficient ranged from 0.1 (case a) to 0.96 (case 4).

By the adjusting of absorption and the extinction coefficients, roughness lengths, and eddy diffusivity, the model produced the correct LST in wet season. Light property and motion characteristics varied in different status of lake. Better results may get based on more observations.

4.3. Validation of Lake-Atmosphere Interaction Processes

The tuned model captured the diurnal variation of temperature (Figure 13). The air temperature ranged from 1.6°C to 29.2°C with an average value of 16.5°C (Figure 13b). The model underestimated diurnal variation of air temperature by nearly 1°C. It was partly because the lake stored more radiation into deeper water and released less into the overlying atmosphere (Figure 14c). The LST varied primarily according to solar radiation. It increased from 9.2°C in January to 24.5°C in August, averaging in 17°C (Figure 13a). Changes in the LST followed and lagged behind its upper atmosphere due to large water thermal capacity. The LST was overestimated during summer because the incoming solar radiation was overestimated, resulting from underestimate of the cloudage.

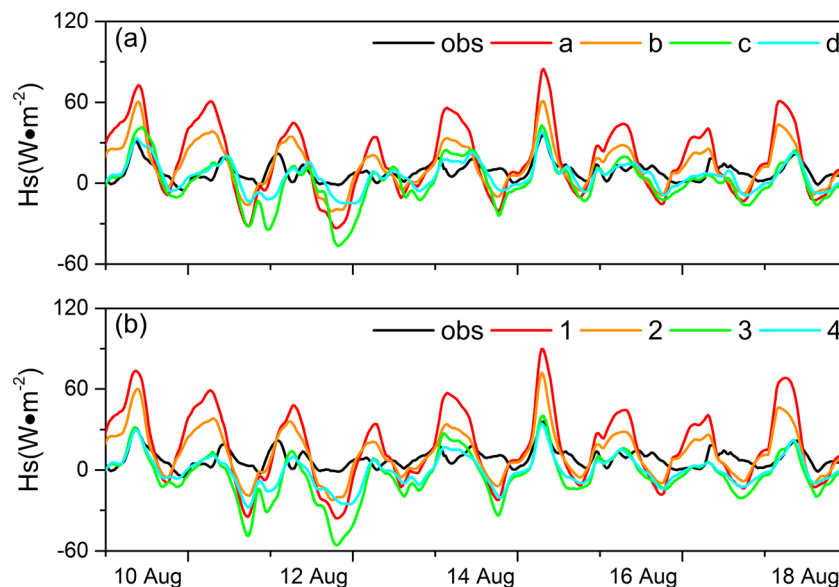


Figure 11. (a and b) Sensible heat flux comparison for observation (obs) and simulations of different model parameter setting in Table 3 (units: W m^{-2}).

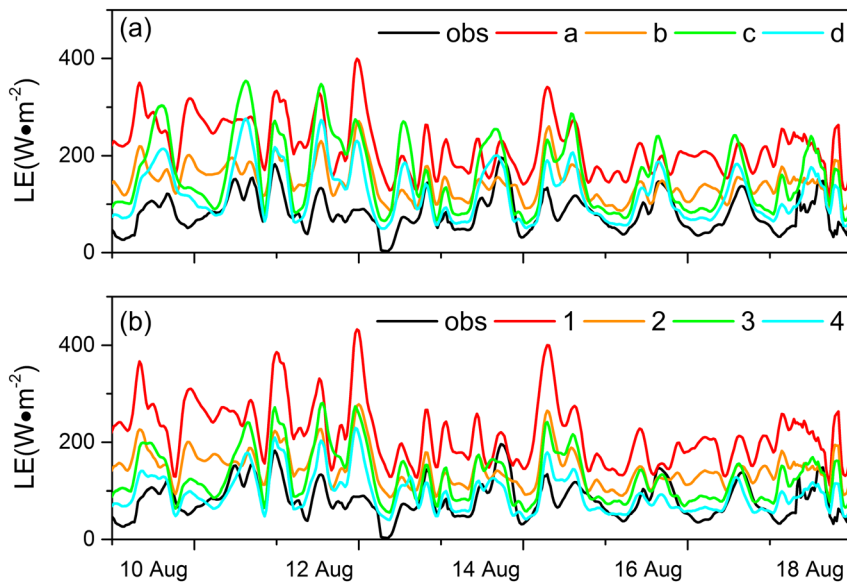


Figure 12. Latent heat flux comparison for observation (obs) and simulations of different model parameter setting in Table 3 (units: W m^{-2}).

The diurnal variation of sensible heat flux was larger in dry season than that in wet season (Figure 14a) because of higher wind speed and larger temperature gradient at that time. Compared to lakes in high latitudes, lakes in low latitudes change energy participation by decreasing sensible heat flux and increasing latent heat flux [Dutra *et al.*, 2010]. The latent heat flux had a larger amplitude (60 W m^{-2} – 150 W m^{-2}) than sensible heat flux but less than the heat storage term (-200 W m^{-2} – 600 W m^{-2}). The model overestimated latent heat flux especially in spring and summer when weather system brought precipitation. It was partly due to the overestimation of wind speed resulting from the smooth of topography when dealt with synoptic-scale atmosphere circulation over complex terrain [Jimenez and Dudhia, 2013]. It is essential to parameterize subgrid topography to appropriate representation of surface wind speed in numerical weather models. Evaporation is larger in the Erhai Lake than that in the Tämnaren Lake [Elo, 2007]. The lake was a heat sink from March to July and served as a heat source from September to January of the next year. It was a transition period in February and August. The heat storage term and latent heat flux dominated heat budget most of the year, while during conversion period latent heat flux was the main part. Large net solar radiation in summer almost balanced with heat storage and latent heat flux.

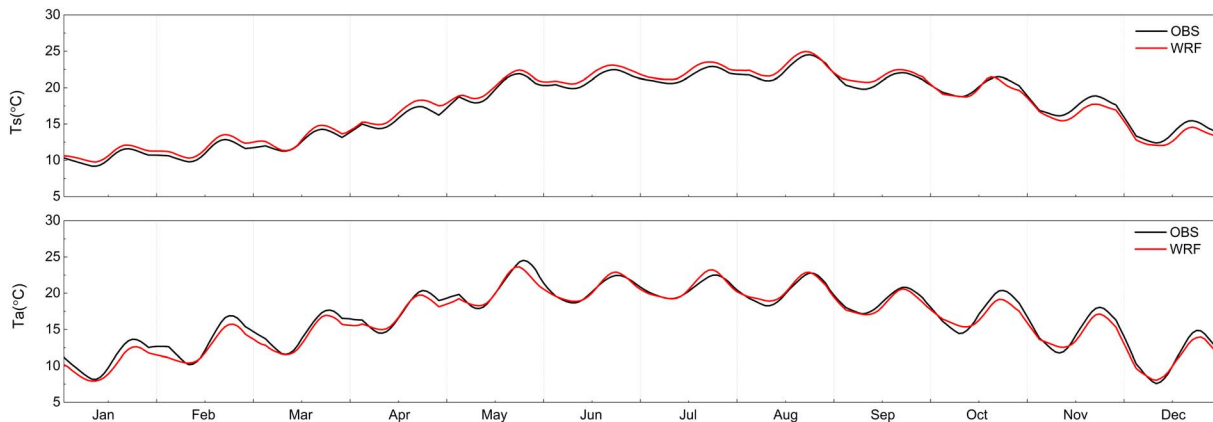


Figure 13. Monthly average diurnal course of (a) lake surface temperature (b) air temperature at 2 m (units: $^{\circ}\text{C}$).

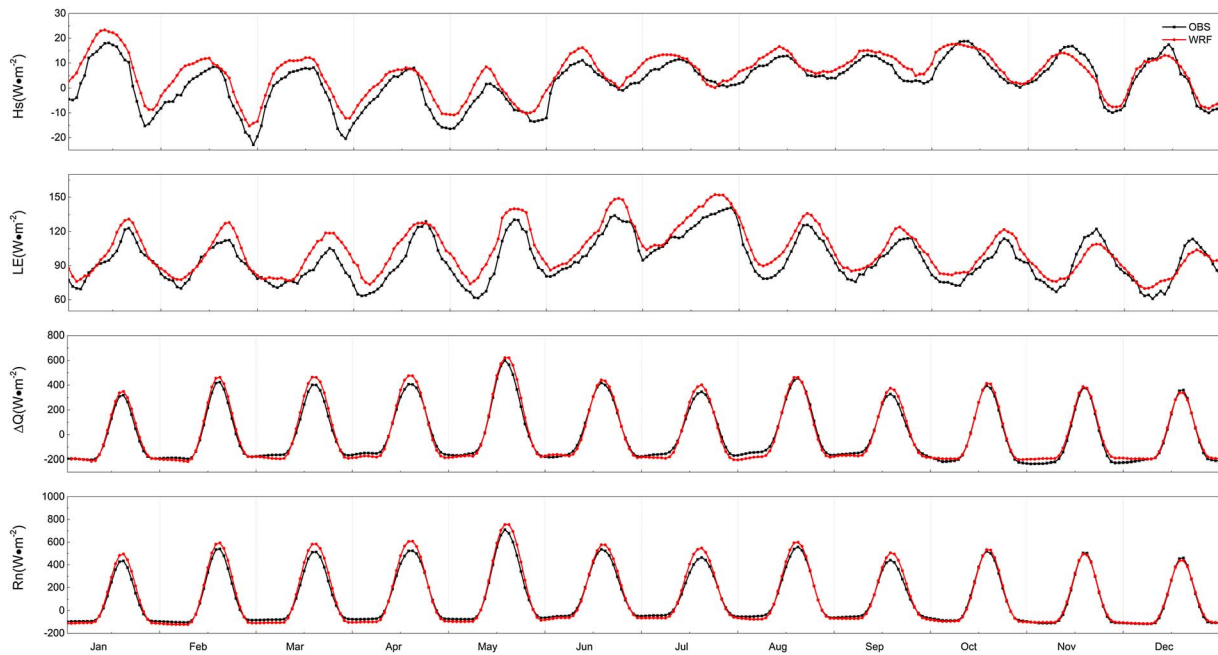


Figure 14. Monthly average diurnal course of (a) sensible heat flux, (b) latent heat flux, (c) heat storage, and (d) net radiation of observation and tuned simulation (units: W m⁻²).

4.4. Topographic Correction

The WRF model overestimated wind speed and turbulent mixing, producing a wetter and lower planetary boundary layer over complex terrain. Previous researches have pointed out that the subgrid-scale orography has important effect on the surface layer wind simulation [Lee et al., 2015; Kalverla et al., 2016]. Following Jimenez and Dudhia [2012], we parameterized the effects of the unresolved terrain as a factor c_t in the momentum conservation equation:

$$\frac{\partial u}{\partial t} = \dots - c_t \frac{u_*^2}{\Delta z} \frac{u}{V}, \quad (12)$$

where u is the zonal wind component, V is the wind speed, u_* is the friction speed, Δz is the thickness of the first model layer, and c_t is given as the following:

$$c_t = \begin{cases} 1 & \text{if } \Delta^2 h > -20 \text{ and } \sigma_{ss0} < e \\ \ln \sigma_{ss0} & \text{if } \Delta^2 h > -10 \text{ and } \sigma_{ss0} > e \\ \alpha \ln \sigma_{ss0} + 1 - \alpha & \text{if } -10 > \Delta^2 h > -20 \text{ and } \sigma_{ss0} > e, \\ \frac{\Delta^2 h + 30}{10} & \text{if } -20 > \Delta^2 h > -30 \\ 0 & \text{if } -30 > \Delta^2 h \end{cases} \quad (13)$$

where $\Delta^2 h$ is the nondimensional Laplacian operator and σ_{ss0} is the standard deviation of subgrid-scale orography. The rest parameters were the same to case 4 in Table 2.

Correction of topography over complex terrain showed distinctive improvement on simulations of the surface layer wind and air-lake surface energy fluxes. There is a clear tendency to reduce wind speed at the Erhai site (Figure 15). The mean bias of wind speed decreased from 0.8 m/s to 0.3 m/s. Lee et al. [2015] used the subgrid-scale orography parameterization and came to the same conclusion. The prevailing wind changed from SE to ESE, which was in consistent with observations. Improvement in surface wind also gave a better representation of surface heat fluxes. Without topographic correction, the R^2 values were 60% and 70% of the sensible and latent heat fluxes. With topographic correction, the WRF model explained 77% and 75%, respectively (Figure 16).

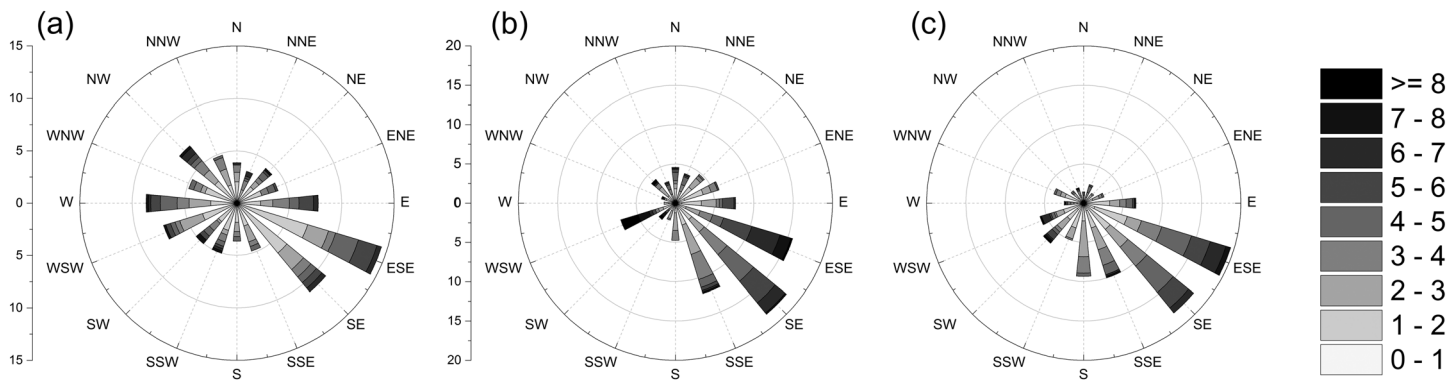


Figure 15. Wind rose at the Erhai site during simulation period (a) observation, (b) WRF without topographic correction, and (c) WRF with topographic correction.

At regional scale, the topographic correction reduced wind speed in simulated area (Figure 17a). This effect was especially evident over leeward slope of mountains. With topographic correction, the sensible heat flux and latent heat flux slightly increased over smooth underlying surface. At leeward slope, it aggrandized sensible heat flux up to 20 W m^{-2} along the mountain ranges. It was partly due to the enlarged temperature difference. The improved representation of the surface wind by the topography correction induced moisture convergence on the leeward side of the mountains. The latent heat fluxes decreased by nearly 10 W m^{-2} on average along the mountain ranges where the moisture difference reduced. The topographic correction in the WRF model reduced wind in the surface layer below 1 km and added wind between 1 and 3 km over leeward of the Cangshan Mountain. It had little impact on atmosphere upper than 3 km. Overall, topographic correction over complex terrain is necessary. It corrects positive wind bias and confines overmuch latent heat exchange.

5. Conclusions and Discussion

The WRF lake model performance on lake-atmosphere interaction at plateau Erhai Lake was evaluated. Radiation forcing drives energy exchange at interface. The RRTMG radiation scheme matched better than other radiation schemes with observations. The default lake model generated negative bias of lake surface temperature. Through a great range of sensitivity tests, we found that the bias in LST simulations result from underestimation of absorption in the surface layer and extinction of solar radiation by lake water. What is more, the roughness length and heat exchange between upper layer and sublayer water through eddy diffusion were dramatically overestimated. Model parameters of the absorption and extinction coefficient are set for clear water. The Erhai Lake is in the stage of midnutrition with a mean spectral extinction

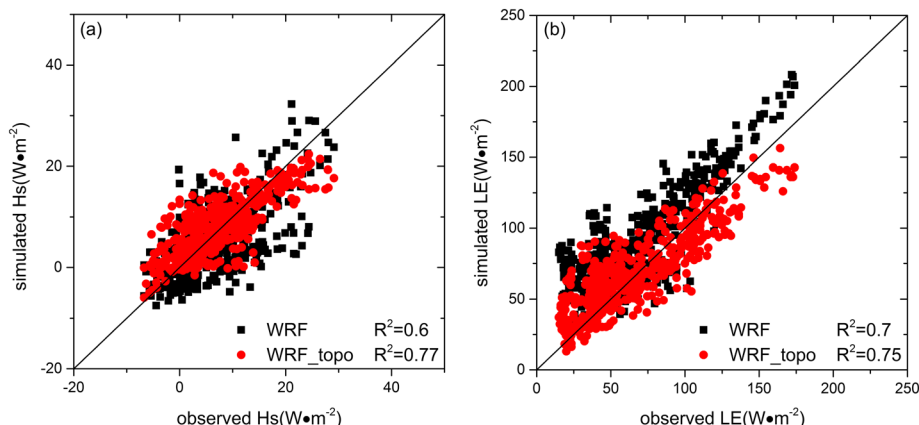


Figure 16. Model predicted surface fluxes versus observations during simulation period of (a) sensible heat flux and (b) latent heat flux (units: W m^{-2}). The black (red) rectangles are WRF without (with) topographic correction.

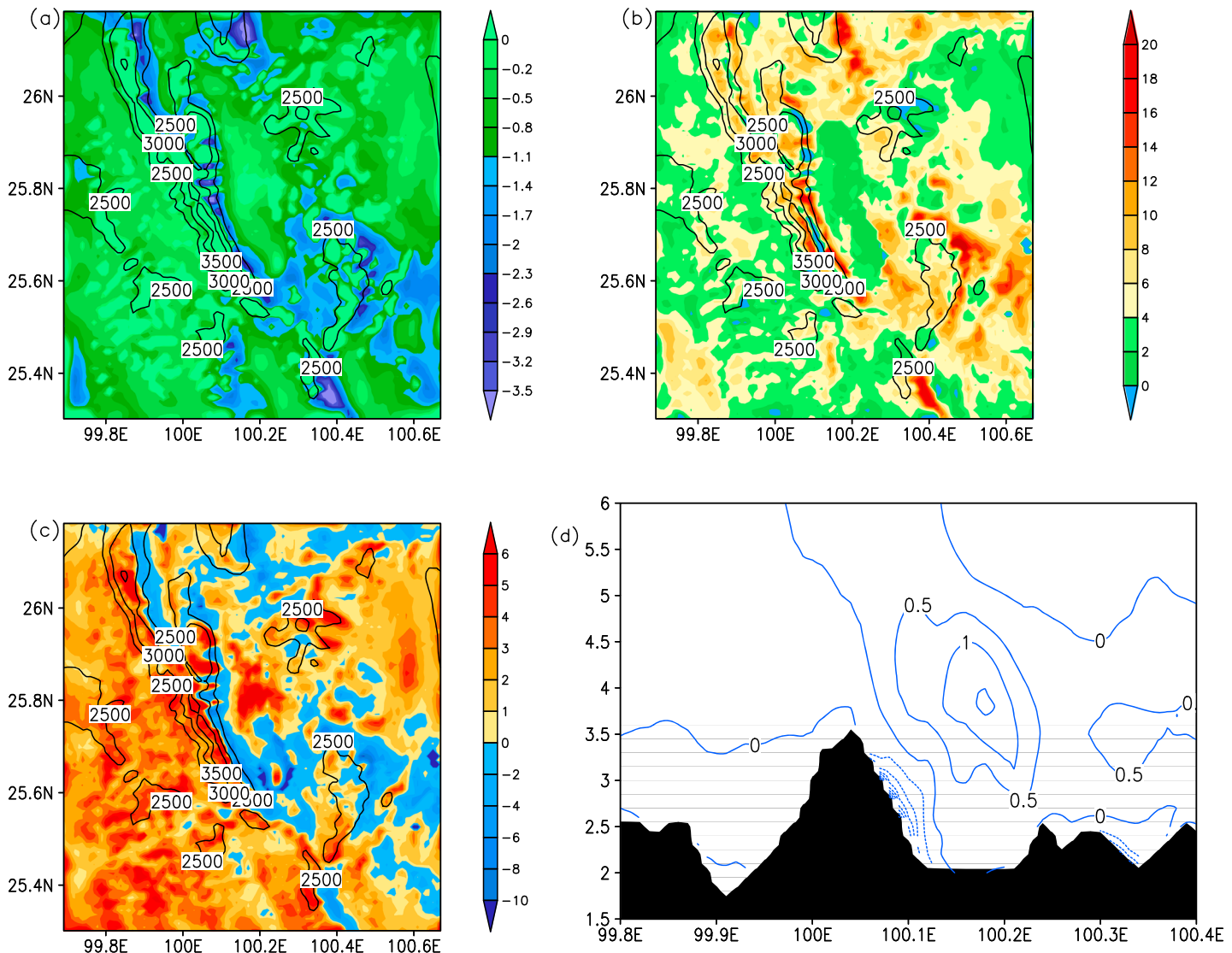


Figure 17. Time-averaged simulated (a) 10 m wind speed, (b) sensible heat flux (units: W m^{-2}), (c) latent heat flux (units: W m^{-2}), and (d) vertical velocity across 25.7°N in the innermost domain (simulation with topographic correction minus simulation without topographic correction). The black solid line indicated the terrain height (units: m).

coefficient of 1.1 m^{-1} in dry season and 2.4 m^{-1} in wet season, resulting absorption coefficient of 0.6 and 0.8, respectively. Parameterization of roughness length showed significantly improvement of LST and heat flux simulations. It is vital to reproduce transport processes of momentum, heat, and water vapor in the surface layer. Ignoring the fact that surface roughness lengths of lakes are substantially smaller than that of other underlying surfaces will lead to large deviations in LST and surface flux prediction. These deviations are larger than the effect of water turbidity.

In Erhai Lake, temperature stratification was stable during daytime, turning to unstable at night. Turbulent mixing by the parameterization of Henderson-Sellers was too strong in shallow lakes. We shrank the eddy diffusion coefficient to impose restrictions on mixing strength in the upper water. Reducing k_e by a factor of 0.05 in dry season and 0.02 in wet season, the simulated LST showed commendable diurnal range with observed temperature.

The WRF model overestimated wind speed and turbulent mixing in the surface layer. Topographic correction was conducted using the method of Jimenez and Dudhia [2012]. It improved performance on wind and surface flux simulations, indicating necessity of topographic correction over complex terrain. Diminishing

of the surface wind led to a weaker mechanical turbulence, resulting in less latent heat exchange. Further studies will adopt the current model results to investigate local flow patterns and its impacts on lake-atmosphere interaction. Although topographic correction improved wind simulation at the Erhai site, it increased surface fluxes with smaller surface wind over windward slope of the Cangshan Mountain. Restrictions for sharp slope in complex mountainous terrain still remain. A better orography parameterization scheme is expected in future studies.

Acknowledgments

This study was supported by funding from the National Natural Science Foundation of China (projects 91537212 and 41321064). We would like to acknowledge the related persons in Dali National Climate Observatory for maintaining the Erhai site. We are also grateful to Yongwei Wang at the Yale-NUIST Center on Atmospheric Environment, Nanjing University of Information Science, China, for her invaluable suggestions. Modeling results and the observational data sets presented in this study are available upon request to the corresponding author (huizhil@mail.iap.ac.cn).

References

- Adrian, R., et al. (2009), Lakes as sentinels of climate change, *Limnol. Oceanogr.*, 54(6), 2283–2297.
- Bartunkova, K., Z. Sokol, and L. Pop (2014), Simulations of the influence of lake area on local temperature with the COSMO NWP model, *Atmos. Res.*, 147, 51–67.
- Bonan, G. B. (1995), Sensitivity of a GCM simulation to inclusion of inland water surfaces, *J. Clim.*, 8(11), 2691–2704.
- Chen, F., and J. Dudhia (2001), Coupling an advanced land surface-hydrology model with the Penn State-NCAR MM5 modeling system. Part I: Model implementation and sensitivity, *Mon. Weather Rev.*, 129(4), 569–585.
- Chen, J. L., M. M. Hu, H. D. Zhou, Y. C. Wang, Y. C. Wang, Y. H. Li, Y. D. Liu, and J. J. Gao (2015), The research on population dynamics and impact factor of phytoplankton during the cyanobacteria bloom in Lake Erhai, *Acta Hydrobiol. Sin.*, 39(1), 24–28.
- Chou, M. D., and M. J. Suarez (1999), A solar radiation parameterization for atmospheric studies NASA Tech. Memo. 15 (10,460), 42 pp., NASA, Washington, D. C.
- Collins, W. D., P. J. Rasch, B. A. Boville, J. J. Hack, and J. R. McCaa (2004), Description of the NCAR Community Atmosphere Model (CAM 3.0), Tech. Note TN-464 + STR, Natl. Cent. for Atmos. Res., Boulder, Colo. [Available at <http://www.ccsm.ucar.edu/models/atm-cam/docs/description/>]
- Curtarelli, M. P., E. H. Alcantara, C. D. Renno, and J. L. Stech (2014), Physical changes within a large tropical hydroelectric reservoir induced by wintertime cold front activity, *Hydrol. Earth Syst. Sci.*, 18(8), 3079–3093.
- Deng, B., S. D. Liu, W. Xiao, W. Wang, J. M. Jin, and X. H. Lee (2013), Evaluation of the CLM4 lake model at a large and shallow freshwater lake, *J. Hydrometeorol.*, 14(2), 636–649.
- Dudhia, J. (1989), Numerical study of convection observed during the winter monsoon experiment using a mesoscale two-dimensional model, *J. Atmos. Sci.*, 46(20), 3077–3107.
- Dutra, E., V. M. Stepanenko, G. Balsamo, P. Viterbo, P. M. A. Miranda, D. Mironov, and C. Schaer (2010), An offline study of the impact of lakes on the performance of the ECMWF surface scheme, *Boreal Environ. Res.*, 15(2), 100–112.
- Elo, P. A. R. (2007), The energy balance and vertical thermal structure of two small boreal lakes in summer, *Boreal Environ. Res.*, 12(5), 585–600.
- Feng, J. W., H. Z. Liu, J. H. Sun, and L. Wang (2016), The surface energy budget and interannual variation of the annual total evaporation over a highland lake in southwest China, *Theor. Appl. Climatol.*, 126(1), 303–312.
- Gerken, T., T. Biermann, W. Babel, M. Herzog, Y. M. Ma, T. Foken, and H. F. Graf (2014), A modelling investigation into lake-breeze development and convection triggering in the Nam Co Lake basin, Tibetan Plateau, *Theor. Appl. Climatol.*, 117(1–2), 149–167.
- Goudsmit, G. H., H. Burchard, F. Peeters, and A. Wuest (2002), Application of k -epsilon turbulence models to enclosed basins: The role of internal seiches, *J. Geophys. Res.*, 107(12), 3230, doi:10.1029/2001JC000954.
- Goyette, S., N. A. McFarlane, and G. M. Flato (2000), Application of the Canadian Regional Climate Model to the Laurentian Great Lakes region: Implementation of a lake model, *Atmos.-Ocean*, 38(3), 481–503.
- Grell, G. A., and D. Devenyi (2002), A generalized approach to parameterizing convection combining ensemble and data assimilation techniques, *Geophys. Res. Lett.*, 29(14), 1693, doi:10.1029/2002GL015311.
- Gu, H. P., X. S. Shen, J. M. Jin, W. Xiao, and Y. W. Wang (2013), An application of a 1-D thermal diffusion lake model to Lake Taihu, *Acta Meteorol. Sin.*, 71(4), 719–730.
- Gu, H. P., J. M. Jin, Y. H. Wu, M. B. Ek, and Z. M. Subin (2015), Calibration and validation of lake surface temperature simulations with the coupled WRF-lake model, *Clim. Change*, 129(3–4), 471–483.
- Haginoya, S., H. Fujii, T. Kuwagata, J. Xu, Y. Ishigooka, S. Kang, and Y. Zhang (2009), Air-lake interaction features found in heat and water exchanges over Nam Co on the Tibetan Plateau, *Sola*, 5, 172–175.
- Haginoya, S., H. Fujii, J. H. Sun, and J. Y. Liu (2012), Features of air-lake interaction in heat and water exchanges over Erhai Lake, *J. Meteorol. Soc. Jpn.*, 90C(2), 55–73.
- Heiskanen, J. J., et al. (2015), Effects of water clarity on lake stratification and lake-atmosphere heat exchange, *J. Geophys. Res. Atmos.*, 120, 7412–7428, doi:10.1002/2014JD022938.
- Hong, S. Y., Y. Noh, and J. Dudhia (2006), A new vertical diffusion package with an explicit treatment of entrainment processes, *Mon. Weather Rev.*, 134(9), 2318–2341.
- Hostetler, S. W., and P. J. Bartlein (1990), Simulation of lake evaporation with application to modeling lake level variations of Harney-Malheur Lake, Oregon, *Water Resour. Res.*, 26(10), 2603–2612.
- Hu, W. F., N. A. Wang, and L. Q. Zhao (2015), Water-heat exchange over a typical lake in Badain Jaran desert, China, *Prog. Geogr.*, 34(8), 1061–1071.
- Iacono, M. J., and T. R. Nehrkorn (2010), Assessment of radiation options in the Advanced Research WRF weather forecast model, in *Proc. First Atmospheric System Research Science Team Meeting*, pp. 15–19, Department of Energy Office of Science, Bethesda, Md.
- Jimenez, P. A., and J. Dudhia (2012), Improving the representation of resolved and unresolved topographic effects on surface wind in the WRF model, *J. Appl. Meteorol. Climatol.*, 51(2), 300–316.
- Jimenez, P. A., and J. Dudhia (2013), On the ability of the WRF model to reproduce the surface wind direction over complex terrain, *J. Appl. Meteorol. Climatol.*, 52(7), 1610–1617.
- Joehnk, K. D., and L. Umlauf (2001), Modelling the metalimnetic oxygen minimum in a medium sized alpine lake, *Ecol. Modell.*, 136(1), 67–80.
- Kalverla, P., G. J. Duine, G. J. Steeneveld, and T. Hedde (2016), Evaluation of the Weather Research and Forecasting model in the Durance Valley complex terrain during the KASCADE field campaign, *J. Appl. Meteorol. Climatol.*, 55(4), 861–882.
- Lee, J. H. H., Shin, S. Y. Hong, P. A. Jimenez, J. Dudhia, and J. Hong (2015), Impacts of subgrid-scale orography parameterization on simulated surface layer wind and monsoonal precipitation in the high-resolution WRF model, *J. Geophys. Res. Atmos.*, 120, 644–653, doi:10.1002/2014JD022747.

- Li, Z. G., S. H. Lyu, L. Zhao, L. J. Wen, Y. H. Ao, and S. Y. Wang (2015), Turbulent transfer coefficient and roughness length in a high-altitude lake, Tibetan Plateau, *Theor. Appl. Climatol.*, 124(3), 1–13.
- Lin, Y.-L., and I. C. Jao (1995), A numerical study of flow circulations in the central valley of California and formation mechanisms of the Fresno eddy, *Mon. Weather Rev.*, 123(11), 3227–3239.
- Liu, H. Z., J. W. Feng, J. H. Sun, L. Wang, and A. L. Xu (2015), Eddy covariance measurements of water vapor and CO₂ fluxes above the Erhai Lake, *Sci. China-Earth Sci.*, 58(3), 317–328.
- Long, Z., W. Perrie, J. Gyakum, D. Caya, and R. Laprise (2007), Northern lake impacts on local seasonal climate, *J. Hydrometeorol.*, 8(4), 881–896.
- Ma, R. H., et al. (2011), China's lakes at present: Number, area and spatial distribution, *Sci. China Earth Sci.*, 41(3), 394–401.
- Masson, V. (2000), A physically-based scheme for the urban energy budget in atmospheric models, *Boundary-Layer Meteorol.*, 94(3), 357–397.
- Mironov, D., E. Heise, E. Kourzeneva, B. Ritter, N. Schneider, and A. Terzhevik (2010), Implementation of the lake parameterisation scheme Lake into the numerical weather prediction model COSMO, *Boreal Environ. Res.*, 15(2), 218–230.
- Mlawer, E. J., S. J. Taubman, P. D. Brown, M. J. Iacono, and S. A. Clough (1997), Radiative transfer for inhomogeneous atmospheres: RRTM, a validated correlated- k model for the longwave, *J. Geophys. Res.*, 102(D14), 16,663–16,682, doi:10.1029/97JD00237.
- Oleson, K. W., et al. (2013), Technical description of version 4.5 of the Community Land Model (CLM), Tech. Note NCAR/TN-503 + STR, 422 pp., Natl. Cent. for Atmos. Res., Boulder, Colo., doi:10.5065/D6RR1W7M.
- Oreopoulos, L., et al. (2012), The continual intercomparison of radiation codes: Results from phase I, *J. Geophys. Res.*, 117, D06118, doi:10.1029/2011JD016821.
- Pan, H., R. Avissar, and D. B. Haidvogel (2002), Summer circulation and temperature structure of Lake Kinneret, *J. Phys. Oceanogr.*, 32(1), 295–313.
- Petenko, I., G. Mastrantonio, A. Viola, S. Argentini, L. Coniglio, P. Monti, and G. Leuzzi (2011), Local circulation diurnal patterns and their relationship with large-scale flows in a coastal area of the Tyrrhenian Sea, *Boundary-Layer Meteorol.*, 139(2), 353–366.
- Ruiz-Arias, J. A., C. Arbizu-Barrena, F. J. Santos-Alamillos, J. Tovar-Pescador, and D. Pozo-Vazquez (2016), Assessing the surface solar radiation budget in the WRF model: A spatiotemporal analysis of the bias and its causes, *Mon. Weather Rev.*, 144(2), 703–711.
- Samuelsson, P., and M. Tjernstrom (2001), Mesoscale flow modification induced by land-lake surface temperature and roughness differences, *J. Geophys. Res.*, 106(D12), 12,419–12,435, doi:10.1029/2001JD900057.
- Samuelsson, P., E. Kourzeneva, and D. Mironov (2010), The impact of lakes on the European climate as simulated by a regional climate model, *Boreal Environ. Res.*, 15(2), 113–129.
- Skamarock, W. C., J. B. Klemp, J. Dudhia, D. O. Gill, D. M. Barker, M. G. Duda, X. Huang, W. Wang, and J. G. Powers (2008), A description of the Advanced Research WRF version 3 Tech. Note NCAR/TN-475 + STR.
- Stepanenko, V. M., S. Goyette, A. Martynov, M. Perroud, X. Fang, and D. Mironov (2010), First steps of a Lake Model Intercomparison Project: LakeMIP, *Boreal Environ. Res.*, 15(2), 191–202.
- Stepanenko, V. M., A. Martynov, K. D. Johnk, Z. M. Subin, M. Perroud, X. Fang, F. Beyrich, D. Mironov, and S. Goyette (2013), A one-dimensional model intercomparison study of thermal regime of a shallow, turbid midlatitude lake, *Geosci. Model Dev.*, 6(4), 1337–1352.
- Subin, Z. M., W. J. Riley, and D. Mironov (2012), An improved lake model for climate simulations: Model structure, evaluation, and sensitivity analyses in CESM1, *J. Adv. Model. Earth Syst.*, 4, M02001, doi:10.1029/2011MS000072.
- Tanentzap, A. J., D. P. Hamilton, and N. D. Yan (2007), Calibrating the Dynamic Reservoir Simulation Model (DYRESM) and filling required data gaps for one-dimensional thermal profile predictions in a boreal lake, *Limnol. Oceanogr.: Methods*, 5, 484–494.
- Thiery, W., V. M. Stepanenko, X. Fang, K. D. Johnk, Z. Li, A. Martynov, M. Perroud, Z. M. Subin, F. Darchambeau, D. Mironov, and N. P. M. Van Lipzig (2014), LakeMIP Kivu: Evaluating the representation of a large, deep tropical lake by a set of one-dimensional lake models, *Tellus, Ser. A*, 66(1), 21390, doi:10.3402/tellusa.v66.21390.
- Verburg, P., and R. E. Hecky (2009), The physics of the warming of Lake Tanganyika by climate change, *Limnol. Oceanogr.*, 54(6), 2418–2430.
- Wang, B., Y. Ma, X. Chen, W. Ma, Z. Su, and M. Menenti (2015), Observation and simulation of lake-air heat and water transfer processes in a high-altitude shallow lake on the Tibetan Plateau, *J. Geophys. Res. Atmos.*, 120, 12,327–12,344, doi:10.1002/2015JD023863.
- Wang, W., et al. (2014), Temporal and spatial variations in radiation and energy balance across a large freshwater lake in China, *J. Hydrol.*, 511, 811–824.
- Xu, A. L., A. H. Zhong, J. H. Sun, and G. R. Gui (2016), Vertical structure characteristic from troposphere to low stratosphere in Dali region over the southeastern margin of Qinghai-Xizang Plateau, *Plateau Meteorol.*, 35(1), 77–85.
- Zhang, Y. L., E. L. Zhang, and M. L. Liu (2009), Spectral absorption properties of chromophoric dissolved organic matter and particulate matter in Yunnan Plateau lakes, *J. Lake Sci.*, 21(2), 255–263.